XIII International Conference on Computational Plasticity. Fundamentals and Applications
COMPLAS XIII
E. Oñate, D.R.J. Owen, D. Peric and M. Chiumenti (Eds)

# SIMULATIONS OF FRACTURE IN CONCRETE BEAMS UNDER BENDING USING A CONTINUUM AND DISCRETE APPROACH

**M. NITKA*, L. SKARZYNSKI* AND J. TEJCHMAN***

*Gdansk University of Technology
Narutowicza 11/12, 80-233 Gdansk, Poland
e-mail: micnitka@pg.gda.pl, lskarzyn@pg.gda.pl, tejchmk@pg.gda.pl

**Key words:** Concrete, Fracture, FEM, DEM, x-ray computed tomography.

**Abstract.** The paper describes two-dimensional meso-scale results of fracture in notched concrete beams under bending. Concrete was modelled as a random heterogeneous 4-phase material composed of aggregate particles, cement matrix, interfacial transitional zones and air voids. Within continuum mechanics, the simulations were carried out with the finite element method based on a isotropic damage constitutive model enhanced by a characteristic length of micro-structure. In addition, the discrete element method was used. The concrete micro-structure in calculations was directly taken from real concrete specimens based on 3D x-ray micro-computed tomography images and 2D images by the scanning electron microscope.

ovides information and instructions for preparing a Full Paper to be included in the Proceedings of *COMPLAS XIII Conference*.

## 1 INTRODUCTION

Fracture is a fundamental phenomenon in concrete material. It is very complex since it consists of main cracks with various branches, secondary cracks and micro-cracks. The fracture process strongly depends upon a heterogeneous structure of materials over many different length scales, changing e.g. in concrete from the few nanometres (hydrated cement) to the millimetres (aggregate particles). In order to properly describe fracture in detail, material micro-structure has to be taken into account since its effect on the global results is pronounced [1].

At the meso-scale, concrete may be considered as a composite material wherein four important phases may be separated: cement matrix, aggregate, interfacial transition zones (ITZs) and macro-voids [2,3]. In particular, the presence of aggregate and ITZs is important since the volume fraction of aggregate can be as high as 70-75% in concrete and ITZs with the thickness of about 50 μm are always the weakest regions in usual concretes, wherein cracking starts (because of their higher porosity). ITZs are a heterogeneous and porous region of the cement paste around aggregate particles which is perturbed by their presence. Two different types of failure exist for ITZs [4]: the ITZ-aggregate separation (related to some delamination processes directly at the aggregate surface) and the ITZ-failure (related to cracking). The accurate understanding of the properties and behaviour of ITZ is one of the most important issues in the meso-scale analyses because damage is initiated in the weakest region and ITZ is just this weakest link in concrete.

The concrete behaviour at the meso-scale may be described with continuum finite element (FE) models [2,3] and discrete models [5,6]. Within discrete methods, the most popular ones are: the classical particle discrete element method (DEM), interface element models with constitutive laws based on non-linear fracture mechanics and lattice methods. The advantage of meso-scale modelling is the fact that it directly simulates micro-structure and can be used to comprehensively study local phenomena at the micro-level such as the mechanism of the initiation, growth and formation of localized zones and cracks which affect the macroscopic concrete behaviour (the concrete behaviour at the meso-scale fully determines the macroscopic non-linear behaviour). The DEM models (if they are enough consistent) might progressively replace experimental tests to study the influence of concrete meso-structure (aggregates size, aggregate shape, aggregate roughness, aggregate/mortar volume, macro porosity, etc.) on the concrete behaviour. The disadvantages are: enormous computational cost and a difficult calibration procedure with respect to geometric and mechanical properties of ITZs.

The main objective of this study is to investigate a complicated fracture process 2D conditions in concrete elements under bending at aggregate level using 2 different approaches: a meso-scale continuum model (based on FEM) and discrete model (based on DEM). In these models, the concrete heterogeneity was characterised by four phases, namely, aggregate grains, cement matrix, ITZs and air voids. The geometry of concrete micro-structure was directly taken from real concrete specimens using 2 high resolution and non-destructive techniques, i.e. 3D x-ray micro-computed tomography and 2D scanning electron microscope (SEM). The FE simulations of tensile deformation were carried out with a simple isotropic continuum constitutive damage model enhanced by a characteristic length of micro-structure by means of a non-local theory [1-3]. The DEM calculations were performed with the three-dimensional spherical discrete element model YADE, which was developed at University of Grenoble [7]. The model demonstrated its usefulness to fracture simulations in concrete [5,6].

The major contribution of the paper are calculation results on concrete fracture under bending by means of 2 meso-scale models based on a continuum and discrete approach, wherein concrete was modelled as the 4-phase material with angularly-shaped aggregate particles. The calculated results were directly compared with the experimental images from an in-situ micro-scale x-ray micro-tomograph test. In the first step, 2D calculations were carried out only in order to check the capability of 2 proposed approaches to describe fracture in concrete with experimentally determined micro-structure. Attention was laid on the crack shape propagating between aggregate particles and the effect of ITZs on the macroscopic concrete response with respect to the strength and crack formation.

## 2. EXPERIMENTAL RESULTS

The concrete was prepared from the ordinary Portland cement, aggregate and water. The mean aggregate diameter was $d_{50}$=2 mm, maximum aggregate diameter $d_{max}$=16 mm and aggregate volume $\beta$=75%. The water to cement ratio was equal to 0.42. The tests were carried out on 2 free-supported rectangular notched concrete beams (height $D$=80 mm, depth $B$=40 mm and length $L$=320 mm) (Fig.1). The notch of the height of $D/10$=8 mm and width of 3 mm was located in the beam mid-span. The average uniaxial compressive strength $f_c$

measured on the cubical concrete specimens 10×10×10 cm$^3$, Young's modulus $E$ and Poisson's ratio $\upsilon$, measured on the cylindrical concrete specimens 15×30 cm$^2$, were equal to: $f_c$=51.81 MPa, $E$=36.1 GPa and $\upsilon$=0.22. The measured tensile strength during bending on the concrete beams 4×4×16 cm$^2$ was $f_t$=3.7-4.3 MPa. The quasi-static beam tests were performed with a controlled notch opening displacement rate (crack mouth opening displacement (CMOD)) of 0.002 mm/min using the loading machine Instron 5569. The CMOD gauge with the length of 5 mm was located in the notch at the beam bottom. The test ended for CMOD=0.10-0.15 mm.

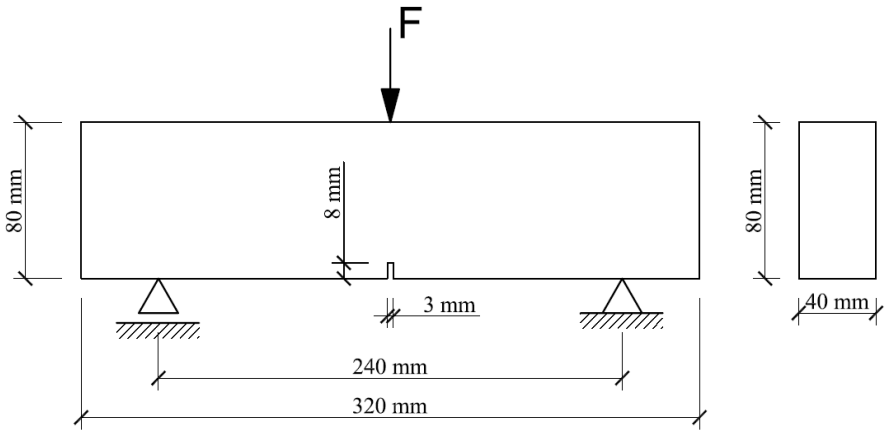


**Figure 1:** Concrete notched beam under quasi-static three-point bending

Two typical experimental diagrams of the vertical force $F$ versus CMOD for the concrete beams of Fig.1 (with the displacement CMOD up to 0.15 mm for the beam '1' and up to 0.10 mm for the beam '2') are shown in Fig.2. The maximum vertical force $F$ was equal to 2.15-2.25 kN (the tensile strength was 3.73-3.91 MPa). After bending tests, the concrete cuboids with the dimensions of 80 mm (height), 50 mm (width) and 40 mm (depth) were cut out from each beam in the notch region for scanning by the $x$-ray micro-tomograph Skyscan 1173 in order to obtain the 3D images of concrete micro-structure (in a damaged state).

Figure 3 demonstrates the 3D images of the cracked cuboidal concrete specimens 80×50×40 mm$^3$ (height×width×depth) which were cut out from the beams in the notch region after each test. The specimen of Fig.3a was cut out from the beam '1' for CMOD≈0.15 mm (when the beam was totally cracked along its height) and the specimen of Fig.3b comes from the beam '2' for CMOD=0.10 mm. The heterogeneous complex 3D concrete micro-structure is well visible on the tomograph images of Fig.3. Three concrete phases (aggregate particles, cement matrix and air voids) may be clearly separated. The measured total volume of air voids was 5.02% (specimen '1') and 4.67% (specimen '2'). The main crack was strongly curved mainly due to a random presence of aggregate grains. Its shape changed along the specimen depth in spite of the fact that 2D boundary value problem (plane stress) was considered. The crack mainly propagated through ITZs (which were the weakest phase in concrete) and sometimes through macro-voids. It might very rarely propagate through a single weak aggregate particle. The crack branching also occurred. The effect of air macro-voids on the crack shape was small.

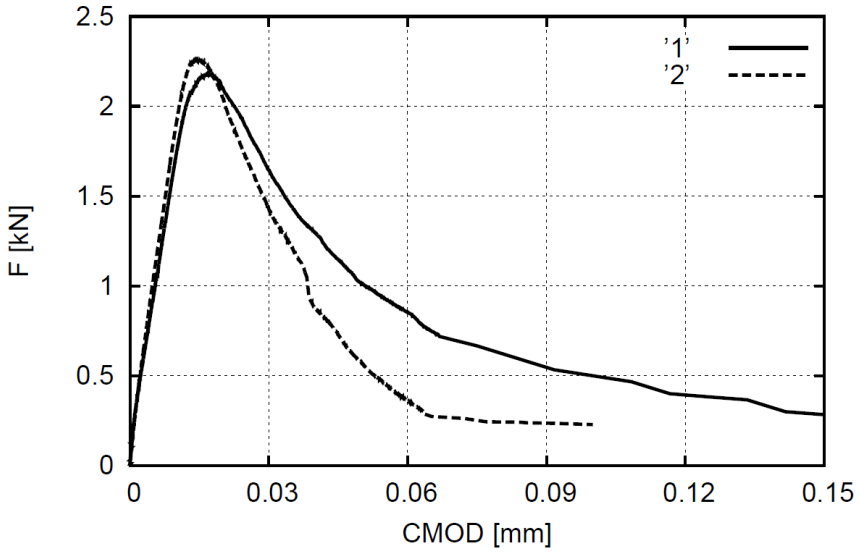


**Figure 2:** Experimental vertical force *F* versus CMOD for two concrete notched beams '1' and '2'

In order to measure the width of ITZs, the scanning electron microscope (SEM) Hitachi TM3030 with the maximum magnification factor 30'000 was used. ITZs around aggregate particles were characterised by a very non-uniform porous structure and presence of separated small sand particles. ITZs appeared mainly aggregate particles but sometimes they were also visible around larger cement matrix particles. The width of ITZs changed between 30-50 μm. The width was not dependent upon the aggregate diameter.

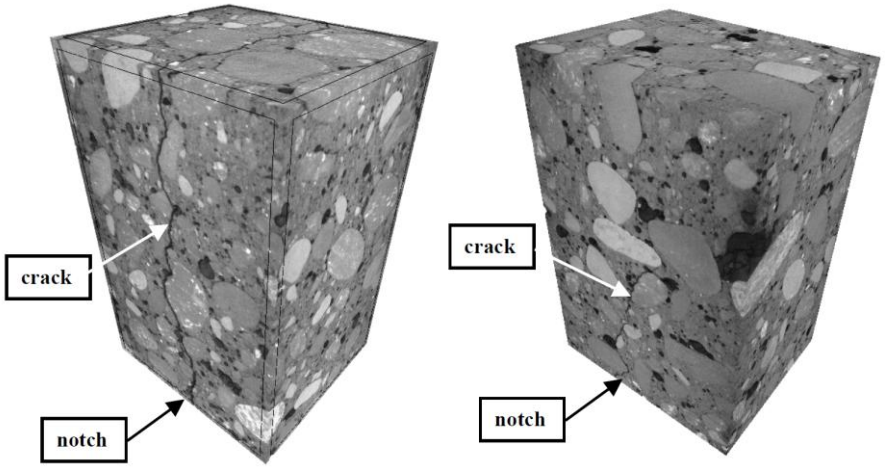


**Figure 3:** Images of cracked cuboidal specimens 80×50×40 mm$^3$ obtained by 3D micro-CT: a) cut out from beam '1' and b) cut out from beam '2' (black spots - voids)

The crack width changed non-linearly with the specimen height from $w_c$=0.75 mm (just above the notch) down to $w_c$=0.22 mm (top) (mid-cross-section of the specimen '1') and from

$w_c$=0.32 mm (just above the notch) down to $w_c$=0.02 mm (top) (mid-cross-section of the specimen '2'). The crack width above the notch varied with the specimen depth from $w_c$=0.45 mm (at the depth of 10 mm from the face side) up to $w_c$=0.75 mm (the mid-sectional cross-section) (specimen '1') and from $w_c$=0.32 mm (at the depth of 5 mm from the face side) down to $w_c$=0.13 mm (at the depth of 35 mm) (specimen '2'). The average crack width in the specimen '1' was $w_c$=0.41 mm wherein the crack propagated through the specimen. In the specimen '2', the average crack width and height were: $w_c$=0.20 mm and $h_c$=50 mm, respectively. The crack height in the specimen '2' changed along the specimen depth, from $h_c$=45 mm (specimen inside) up to $h_c$=56 mm on the front specimen side. The width of the localized zone above the notch on the beam surface, measured by DIC, was $w_{lz}$=3.11-3.40 mm [8].

## 3. MODELS FOR CONCRETE

### 3.1 Continuum constitutive model

A simple isotropic damage continuum model was assumed for calculations with FEM [1-3]. In order to define the equivalent strain measure $\tilde{\varepsilon}$, a Rankine failure type criterion was assumed [9]. To describe the evolution of the damage parameter $D$, the exponential softening law was used [10]. The constitutive isotropic damage model for concrete requires the following 5 constants: $E$ - the modulus of elasticity, $\upsilon$ - the Poisson's ratio, $\kappa_0$ - the initial value of the damage parameter (responsible for the strength) and $\alpha$ and $\beta$ - the softening parameters. The model is suitable for tensile failure.

To properly describe strain localization, to preserve the well-possedness of the boundary value problem and to obtain mesh-independent results, a non-local theory was used as a regularization technique [1-3,11]. In the calculations, the equivalent strain measure $\tilde{\varepsilon}$ was replaced by its non-local value [1-3]. As a weighting function $\omega$, a Gauss distribution function was used [1]. The concrete heterogeneity in the region close to the notch was characterised by four phases: angularly-shaped aggregate particles, cement matrix, ITZs and air voids. The width of the meso-region was equal to 50 mm and was equal to the width of the cuboidal specimens of Fig.3 (Fig.4). In the remaining region, the material was described as the elastic one-phase material ($E_{macro}$=36.1 MPa and $\upsilon_{macro}$=0.2). The aggregates ($d$>1.4 mm), embedded in the cement matrix, were described by a linear elastic model. The location, shape, size and distribution of aggregate grains and air voids for both beams directly corresponded to the concrete images in 3 different cross-sections of Fig.3. The width of ITZs around aggregate particles was constant - 0.05 mm. The FE-mesh included in total 100'000 triangular elements (4 triangles formed a quadrilateral element). The size of finite elements was 0.025-0.2 mm (aggregate), 0.025-0.2 mm (cement matrix) and 0.025 mm (ITZs). The air voids (with the diameter ≥0.8 mm and the total surface of approximately 2.5%) were modelled as the empty spots. The calculations were carried out under plane stress conditions by taking the depth of the beam into account $B$=40 mm when calculating the vertical force.

The following parameters were assigned to each individual phase: aggregate ($d$=1.4-16 mm) ($E_{agg}$=47.2 GPa, $\upsilon$=0.2), cement matrix ($E_{cm}$=29.2 GPa, $\upsilon$=0.2, $\kappa_{0,cm}$=1.5×10$^{-4}$, $\alpha$=0.95, $\beta$=200) and ITZ ($E_{ITZ}$=14.6 GPa, $\upsilon$=0.2, $\kappa_{0,ITZ}$=1.1×10$^{-4}$, $\alpha$=0.95, $\beta$=200). The modulus of elasticity of aggregate grains (composed of 55% of granite, 30% of limestone, 13% of

sandstone and 2% of basalt) was calculated as the mean value of the moduli of the individual components. The modulus of elasticity of the cement matrix was assumed as $E_{cm}$=29.2 GPa and the parameter $\kappa_0$=1.5×10$^{-4}$ based on the own tests. The parameters $\alpha$ and $\beta$ for the cement matrix and ITZs were adjusted to the experimental curves to realistically reproduce material softening in Fig.2. The mesoscopic characteristic length was always assumed $l_c^m$=1.5 mm, based on own experiments on concrete-beams using the digital image correlation technique DIC [8].

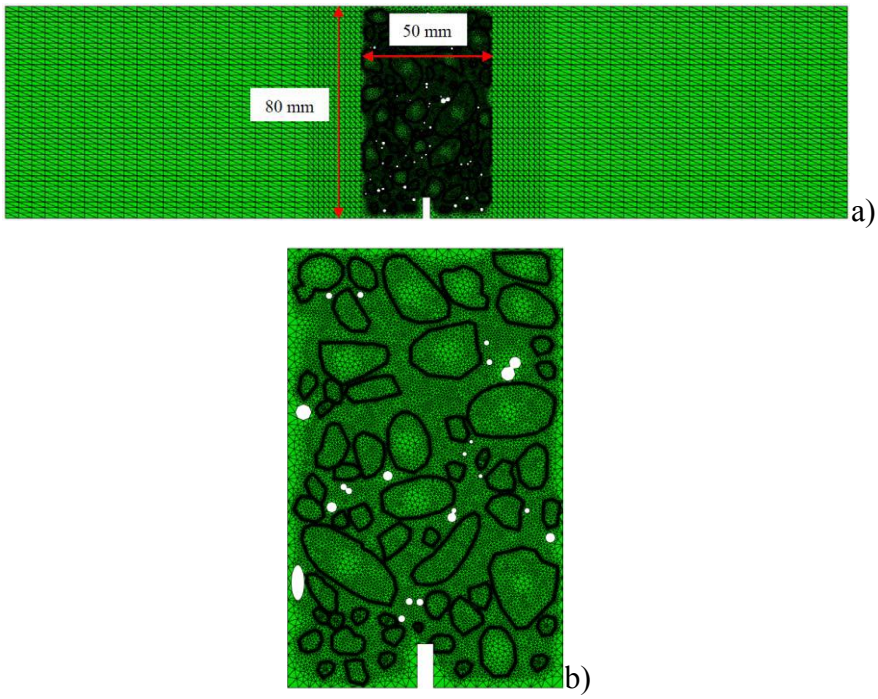


**Figure 4:** 2D FE mesh generated for concrete notched beam '2' of Fig.1: a) entire beam and b) meso-region 50×80 mm$^2$ close to notch based on tomograph image of Fig.3 (specimen mid-sectional cross-section) (white spots - voids)

### 3.1 Discrete element method

The 3D spherical discrete element model YADE takes advantage of the so-called soft-particle approach (i.e. the model allows for particle deformation which is modelled as an overlap of particles) [7]. A linear normal contact model under compression was used. Aggregate grains were modelled as clusters composed of spheres. The interaction force vector representing the action between two spherical discrete elements in contact was decomposed into a normal and tangential vector, respectively. The normal forces acting on spheres were modelled by an elastic law with cohesion. The normal and tangential forces were linked to the displacements through the normal stiffness $K_n$ and the tangential stiffness $K_s$. The stiffness parameters were computed with the aid of the modulus of elasticity of the grain contact $E_c$ and two neighbouring grain radii $R_A$ and $R_B$ (to determine the normal stiffness $K_n$) and with the aid of the modulus of elasticity $E_c$ and Poisson's ratio $\upsilon_c$ of the grain contact and two neighbouring grain radii $R_A$ and $R_B$ (to determine the tangential stiffness $K_s$), respectively [7].

The contact tangential forces $\vec{F}_s$ and normal forces $\vec{F}_n$ satisfied the cohesive-frictional Mohr-Coulomb equation using the inter-particle friction angle $\mu$ [7]. The normal force might be negative down to the minimum value of $F_n^{\min}$ if there was no a geometrical contact between elements. If this minimum normal force between spheres $F_n^{\min}$ was reached, the contact was broken. Moreover, if any contacts between grains re-appeared, cohesion between them was not taken into account. A crack was considered as open if cohesive forces between grains disappeared when a critical threshold was reached. A choice of a very simple linear elastic normal contact was intended to capture on average various contact possibilities in real concrete. One assumed that the cohesive force and tensile force were a function of the cohesive stress $C$ (maximum shear stress at pressure equal to zero), tensile normal stress $T$ and sphere radius $R^2$ [6]. To dissipate excessive kinetic energy in a discrete system, a simple local non-viscous damping scheme was adopted which assumed a change of forces by using the damping parameter.

The following 5 main local material parameters were needed for our discrete simulations: $E_c$, $\upsilon_c$, $\mu$, $C$ and $T$ which may be successfully calibrated with real laboratory uniaxial tests on compression and tension of concrete specimens [6]. In addition, the particle radius, particle mass density and damping parameters are required.

In DEM computations of the concrete beam as a four-phase material, aggregates ($d$=2-16 mm) were modelled as grain clusters with the diameter of $d$=0.5 mm connected to each other as rigid bodies (Fig.5). One aggregate particle, depending upon its diameter, included 10-500 cylinders. All aggregate grains ($d$>2 mm) included ITZs. The aggregate volume was 75%. The cement matrix was modelled with the spheres with the diameter $d$=0.25-2 mm without ITZs. The cement matrix grains filled the concrete specimen in 95% [6]. The macro air voids ($d$>0.8 mm) where assumed as the empty spaces. The remaining beam region (outside the meso-region close to the notch) was simulated with the spheres of $d$=2-8 mm (Fig.5). In order to significantly shorten the computations, the beam included only one layer of grains [6] for 2D calculations. For the sake of simplicity, ITZs were solely simulated as the contacts between aggregate and cement matrix grains (thus they had a no physical width).

Based on preliminary calculations of uniaxial compression [6], uniaxial tension [6] and triaxial compression tests, the following parameters of cohesion and tensile strength were assigned to the cement matrix ($E_{c,cm}$=29.2 GPa, $C_{cm}$=140 MPa and $T_{cm}$=25 MPa) and ITZs ($E_{c,ITZ}$=20.4 GPa, $C_{ITZ}$=100 MPa and $T_{ITZ}$=17.5 MPa). Note that there were no contacts between aggregate grains. In the remaining region outside the meso-region with large grains was described by the constants: $E_{macro}$=36.1 GPa, $C_{macro}$=140 MPa and $T_{macro}$=25 MPa.

The contact elastic stiffness of the cement matrix and beam macro-zone were taken directly from laboratory tests (i.e. they were the same as in the FEM calculations). The remaining material parameters were constant for all phases and regions: $\upsilon_c$=0.2 (Poisson's ratio of grain contact), $\mu$=18$^o$ (inter-particle friction angle), $\alpha_d$=0.08 (damping parameter) and $\rho$=2.6 kG/m$^3$ (mass density). The inter-particle friction angle was assumed based on triaxial compression tests with granulates in the form of clumps [12]. The material constants $C$ i $T$ were adopted with the aid of the uniaxial compression test (2D concrete specimen 10×10 cm$^2$) and bending test (2D concrete specimen 4×16 cm$^2$) with concrete through a comparison between experiments and numerical outcomes [6]. With the assumed material properties and

grain size distribution curve, the DEM calculations provided the uniaxial compressive strength of 49.5 MPa, the compressive elastic modulus of 36 GPa and the tensile strength during bending of 4.40 MPa (2D concrete specimen 4×16 cm$^2$), i.e. similarly as in the experiments ($f_c$=51.81 MPa, $f_t$=4.04 MPa, $E$=36.1 GPa and $f_t$=3.7-4.3 MPa).

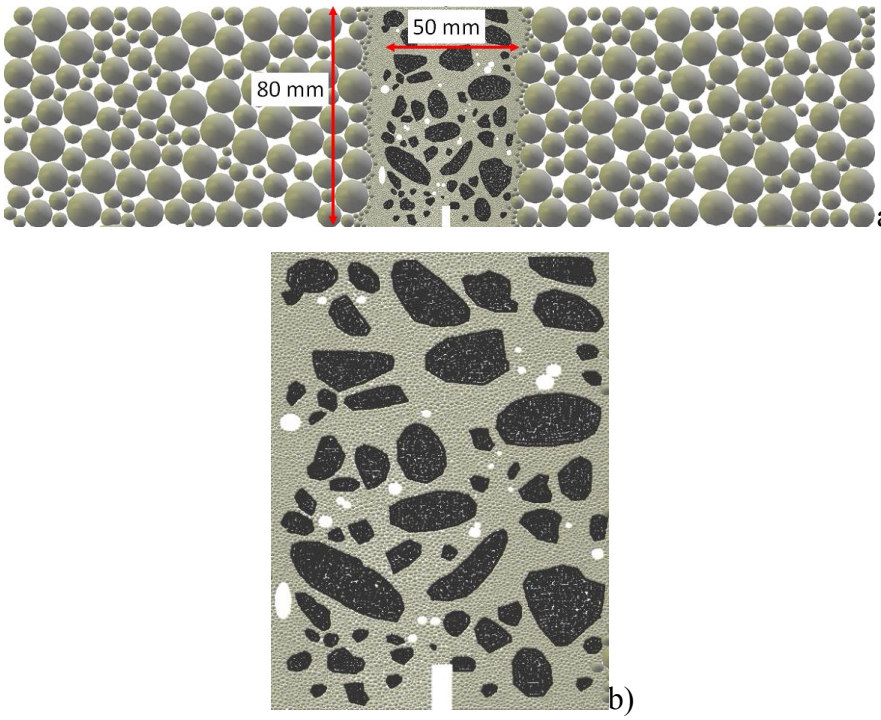


**Figure 5:** 2D DEM grain geometry for concrete beam '2': a) entire beam and b) meso-region close to notch of 50×80 mm$^2$ based on tomography image of Fig.3 (mid-sectional cross-section) (white spots - voids)

The beam included in total about 25'000 grains (20'000 grains in the meso-region with $d_{min}$=0.25 mm) (Fig.5). Each concrete beam was constructed in a simple way by putting grain clusters in the position of aggregate in the beam meso-region. Next the cement matrix grains were randomly added to the meso-region with the inter-granular friction angle equal to $\mu$=0$^o$ in order to obtain a relatively dense specimen. The beam macro-region was filled up with the spheres of the beam of $d$=2-8 mm with $\mu$=0$^o$. The entire assembly was then allowed to settle to a state when the kinetic energy was negligible and then all contact forces between spheres were deleted. In the places where macro air voids existed, the grains were deleted. Before the beam was loaded, the parameters $C$, $T$ and $\mu$ given in Tab. 3 were imposed. Afterwards the element assembly was subjected to deformation. The constant vertical velocity $v$=2 mm/s was applied at the place of $F$. The imposed damping factor and the velocity of the prescribed displacement did not affect the results [6].

## 4. NUMERICAL RESULTS

Figures 6 demonstrate the force-CMOD curves obtained for the concrete beams '1' and '2' with the real aggregate and air voids distribution in three different cross-sections of Figs. 6A

and 6B in the notch region using FEM and DEM. The calculated (FEM) and experimental force-CMOD curves are very similar in the entire hardening-softening regime. The calculated maximum vertical force was $F$=2.08-2.22 kN for CMOD=0.16-0.20 (beam '1') and $F$=2.31-2.37 kN (beam '2') for CMOD=0.017-0.23 mm in 3 different vertical cross-sections. In the experiments, the maximum vertical force was $F$=2.15 kN (beam '1') for CMOD=0.017 mm and $F$=2.25 kN (beam '2') for CMOD=0.016 mm. The residual vertical forces were also similar in the calculations and experiments. Thus, the agreement of the curves $F$=f(CMOD) between FEM and experiments was very good.

In the DEM computations the agreement of the curve $F=f$(CMOD) with the experiments was slightly worse (in particular in the mid-sectional cross-sections in the beam '2'). The calculated maximum vertical force was $F$=2.11-2.21 kN for CMOD=0.014-0.015 mm (beam '1') and $F$=2.22-2.70 kN for CMOD=0.015-0.016 mm (beam '2'). The calculated residual forces were similar in the beam '1' and higher by 20-100% in the beam '2'. As compared to FEM, the calculated forces versus CMOD indicated clear fluctuations after the peak.

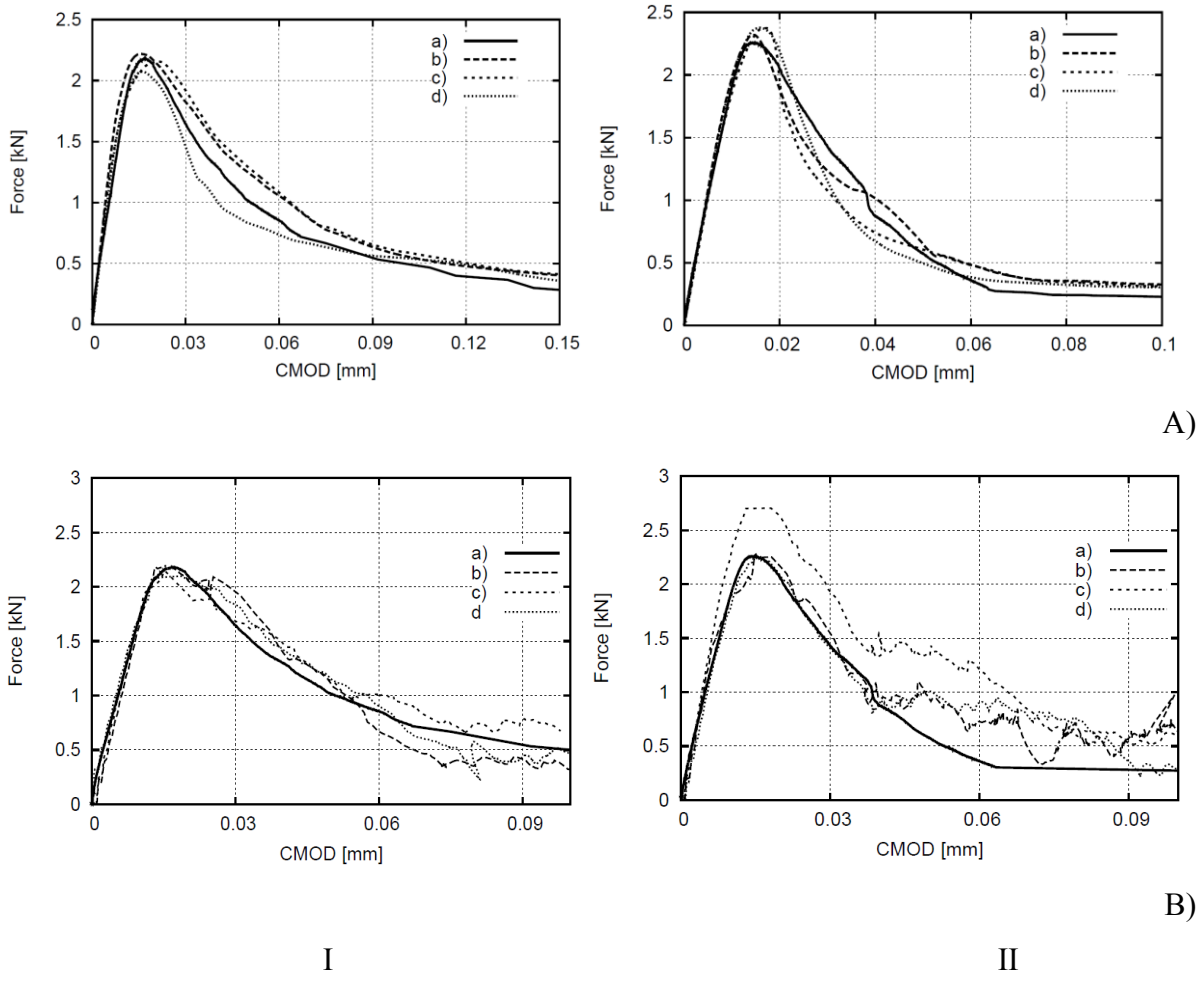


**Figure 6:** Evolution of vertical force against CMOD from FEM (A) and DEM (B): a) experimental curves, b-d) calculated curves for concrete micro-structure (beam '1' (I) and beam '2' II)

The shape, height and location of the localized zone in FEM based on the distribution of the non-local strain measure (Fig.7b) and the crack in DEM based on the broken grain contacts (when the minimum normal force between spheres $F_n^{\min}$ was reached) (Fig.7c) are in satisfactory agreement with the experimental outcomes based on μCT images (Fig.3).

The localized zone always propagated in FEM through ITZs and sometimes by macro air voids (Fig.7c). The localized zone was created before the peak on the vertical force-CMOD diagram for 90%-95% of $F_{max}$. It appeared as a single slightly curved zone which mainly developed in the CMOD range of 0.013-0.06 mm. The maximum calculated length and height of the localized zone above the notch (beam '2') were: $l_{lz}$=58-59 mm and $h_{lz}$=53-56 mm ($h_{lz}/D$≈0.66-0.70). In order to determine the width of the localized zone $w_{lz}$, the calculated displacements were fitted by the error function ERF [8]. The calculated width of the localized zone width above the notch was $w_{lz}$=3.38-3.85 mm ((2.25-2.56)×$l_c^m$) (CMOD=0.05 mm) for the beam '1' and '2' – similarly as in the experiments with DIC $w_{lz}$=3.11-3.40 mm [8]. The zone width changed along the beam height. Its largest width was $w_{lz}$=4.5 mm (3×$l_c^m$ at the height of $h$=30 mm, beam '1') – in the experiment $w_{lz}$=4.2 mm [8]. The shape of the localized zone in FEM was identical in some cross-sections as in the experiments (Figs.7Ab and 7Cb) and slightly different in the other beam cross-sections (Fig.7Bb). Some discrepancies occurred mainly in the beam mid-part and beam upper part (in the neighbourhood of small aggregate grains). The numerical localized zone had sometimes a different direction around the same grains.

The shape of the crack in DEM was also similar as in the experiments; the crack propagated again mainly through ITZs and sometimes by macro air voids (Fig.7). The maximum calculated length and height of the crack above the notch (beam '2') were: $l_{lz}$=59.6-63.0 mm and $h_{lz}$=51.3-53.1 mm ($h_{lz}/D$≈0.71-0.74). However, some differences with respect to the propagation way appeared. In the mid-section of the beam '2' (Fig.7Bc), the way of the calculated crack was different from the same beginning. Sometimes the calculated crack run around the different side of small aggregate particles. One also could observe clear crack branches in some points (e.g. in the beam '2', Figs.7B and 7C), similarly as in the experiments. Some single contacts also broke down away from the main crack.

## 5. CONCLUSIONS

Two different 2D meso-scale models were developed based on high-resolution x-ray micro-tomography images to simulate fracture processes in concrete beams under three-point bending. The calculation 2D results for four-phase concrete at aggregate level using an isotropic damage continuum model enhanced by a characteristic length of micro-structure and discrete element model showed satisfactory quantitative agreement with experimental observations. DEM presented significant perspectives to follow in detail the fracture development including micro- and macro-cracks.

The experimental crack above the notch was strongly curved and depended on concrete micro-structure. It mainly propagated through the weakest contact zones (ITZs) between the cement matrix and aggregates. The width of ITZs varied between 30 and 50 μm. Their porosity was strongly uniform. The crack might rarely propagate through a weak aggregate particle. Some small crack branches were also visible. The crack shape was different along the beam depth.

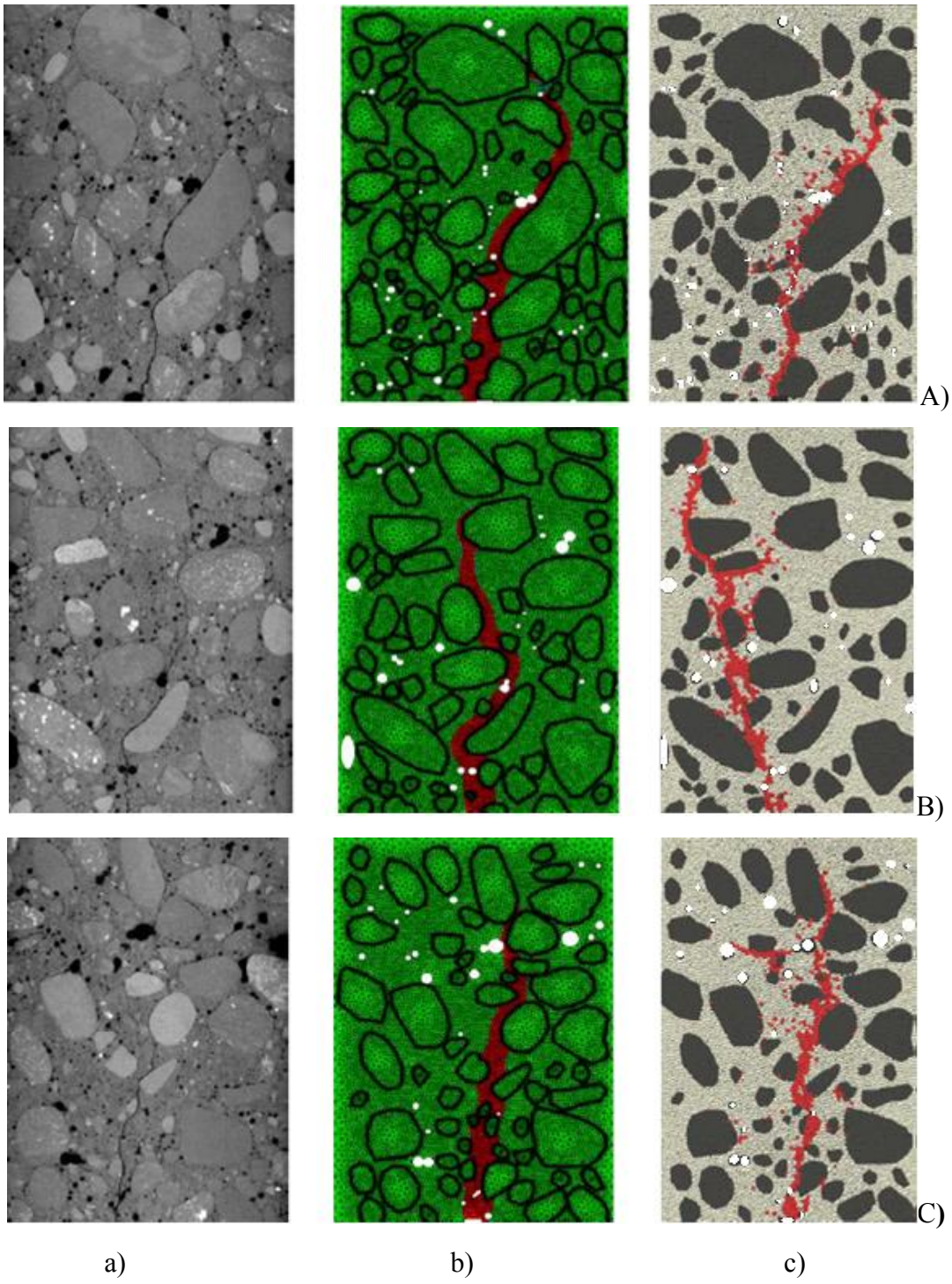


**Figure 7:** Fracture in concrete beam '2' above notch: a) experiments (images by micro-CT after test for CMOD=0.15 mm), b) distribution of non-local strain measure in FEM (CMOD=0.10 mm) and c) breakage of contacts in DEM (CMOD=0.10 mm), A) at depth of 3 mm, B) at depth of 20 mm (mid-region) and C) at depth 37 mm from front beam surface of Fig.3

The mechanical properties of ITZs have a pronounced influence on the material strength and macro-cracking that demonstrates the necessity of their experimental investigations, 3D modelling and small grain presence in DEM computations.

**Acknowledgements**

The research work has been carried out within the project: "*Innovative ways and effective methods of safety improvement and durability of buildings and transport infrastructure in the sustainable development*" financed by the European Union (POIG.01.01.02-10-106/09-01) and the project "*Experimental and numerical analysis of coupled deterministic-statistical size effect in brittle materials*" financed by National Research Centre NCN (UMO-2013/09/B/ST8/03598).

**REFERENCES**

[1] Tejchman, J. and Bobiński, J. *Continuous and discontinuous modelling of fracture in concrete using FEM*. Springer, Berlin-Heidelberg (eds. W. Wu and R. I. Borja) (2013).
[2] Gitman, I.M., Askes, H. and Sluys, L.J. Coupled-volume multi-scale modelling of quasi-brittle material. *Eur. J. Mech. A/Solids* (2008) **27**:302-327.
[3] Skarżyński, Ł. and Tejchman, J. Calculations of fracture process zones on meso-scale in notched concrete beams subjected to three-point bending. *Eur. J. Mech. A/Solids* (2010) **29**:746-760.
[4] Königsberger, M., Pichler, B. and Hellmich Ch. Micromechanics of ITZ-aggregate interaction in concrete Part II: strength upscaling. *J. Amer. Cer. Soc.* (2014) **97**:543-551.
[5] Hentz, S., Daudeville, L. and Donze, F. Identification and validation of a Discrete Element Model for concrete. *J. Engng Mech.* ASCE (2004) **130**:709-719.
[6] Nitka, M. and Tejchman, J. Modelling of concrete behaviour in uniaxial compression and tension with DEM. *Granular Matter* (2015) **17**:145-64.
[7] Kozicki, J. and Donze, F. A new open-source software developer for numerical simulations using discrete modeling methods. *Comp. Meth. in Appl. Mech. Engng.* (2008) **197**:4429-4443.
[8] Skarżyński, Ł. and Tejchman, J. Experimental investigations of fracture process in plain and reinforced concrete beams under bending. *Strain* (2013) **49**:521-543.
[9] Jirásek, M. and Marfia, S. Non-local damage model based on displacement averaging, *Int. J. Num. Meth. Engng* (2005) **63**:77-102.
[10] Peerlings, R.H.J., de Borst, R., Brekelmans, W.A.M. and Geers, M.G.D. Gradient enhanced damage modelling of concrete fracture. *Mech. Coh. Frict. Mat.* (1998) **3**:323-342.
[11] Bažant, Z.P. and Jirásek, M. Non-local integral formulations of plasticity and damage: survey of progress. *J. Engng. Mech.* (2002) **128**:1119-1149.
[12] Kozicki, J., Tejchman, J. and Mróz, Z. Effect of grain roughness on strength, volume changes, elastic and dissipated energies during quasi-static homogeneous triaxial compression using DEM. *Granular Matter* (2012) **14**:457-468.